

A GIS-based weights-of-evidence model for mineral potential mapping of hydrothermal gold deposits in Torbat-e-Heydarieh area

H. Shahi^{1*}, A. Kamkar-Rouhani²

1. PhD Candidate, School of Mining, Petroleum & Geophysics Engineering, University of Shahrood, Shahrood, Iran
2. Associated Professor, School of Mining, Petroleum & Geophysics Engineering, University of Shahrood, Shahrood, Iran

Received 19 May 2012; received in revised form 27 August 2014; accepted 6 September 2014
*Corresponding author: hssn.shahi@gmail.com (H. Shahi).

Abstract

The method of weights of evidence is one of the most important data-driven method for mineral potential mapping in GIS. In this method, considering the characteristics of known mineralized locations, new mineralized areas can be prospected. In this study, the method of weights of evidence was used for hydrothermal gold potential mapping in Torbat-e-Heydarieh area, east of Iran. As a relatively large number of gold mineral occurrences (i.e., exactly 27 known gold mineralized locations) have been recognized in the study area, the use of the weights of evidence method for prospecting new gold mineralized zones in the area can be quite efficient. To determine probable gold mineralization zones in the form of a posteriori map of the survey area, based on weights of evidence method, this study combined the results of the airborne geophysical, geological, argillic, propylitic and iron oxide alteration, geochemical and structural data were. Consequently, four major zones in this area were identified as high gold mineralization potential zones, in which many vein and veinlet mineralization forms can be found.

Keywords: *Geographic Information System (GIS), Gold Mineralization, Weights-of-Evidence Model, Mineral Potential Mapping, Conditional Probability.*

1. Introduction

There are high mineral potentials and a multitude of discovered minerals in Iran. One of the gold and copper mineralization areas in Iran is the study area in Torbat-e-Heydarieh, East of Iran, located in the eastern continuation of Taknar mineralization zone, and is bounded by Darouneh and Rivash faults [1]. In the study area, various kinds of mineralization can be seen that may or may not be accompanied by gold mineralization with different concentrations. The mineralization is generally formed of specularite + quartz \pm chalcopyrite \pm pyrite \pm malachite \pm hematite + gold [1].

Weights of evidence (WOFE) method in GIS was used to prospect gold mineralization zones in the study area, to integrate the results obtained from geological, geochemical and airborne geophysical surveys as well as remote sensing and ground structural investigations. Spatial associations

between mineral occurrences and exploration features can be quantified by the weights of evidence method using the contrast value, which increases with the strength of the spatial relationship. The WOFE method is popular, especially among practitioners who favor an empirical, data-driven approach to prospectivity [2].

As a result, the gold mineralization zones with different mineralization post probability values were recognized in the study area. The results demonstrate the capability of WOFE method for recognition of mineralization zones.

2. Geological description of the study area

The study area is located in Taknar zone, which is uplifted in the form of a wedge block in north of Darouneh fault. The Taknar mineralization zone is underlain by Precambrian and Paleozoic

basement, and overlain by Mesozoic and Cenozoic cover. There are facial and structural differences between this zone and adjacent zones. This zone is limited by two major faults: Darouneh fault in south and Rivash or Taknar fault in north, both faults are of slip-strike type and have an approximate east-west trend [1].

Volcanic activities during Tertiary in east of the Taknar zone, between Darouneh and Taknar faults, start with dark grey tuffs, occasionally of ignimbrite type, accompanied with andesitic black lavas. On this unit, we can see a large thickness of white breccia tuffs, volcanic breccias, grey sandy tuffs, ignimbrites and lapilly tuffs. Andesitic lavas are also formed at the same time with the tuffic activities. In east of Torbat-e-Heydarieh geological map, this set of units is accompanied with conglomerates, which are overlain discontinuously on Cretaceous sediments. In the south of Hesar village, the conglomerates are overlain on the set of units with the same dip. To the east, these conglomerates were changed to sandstone, volcanic breccias, and sand tuffs with andesitic and trachy andesitic lavas. In northeast of Alishir mountain, trachy andesites, having porphyry texture, were observed. The last product of the volcanic activities in this time period is pyroxene, andesite, alkali basalt and trachy andesite in north of Khosh Darreh (east of study area). This set has porphyry and glomero-porphyry texture in which pyroxene and olivine minerals are found in a background composed of plagioclases and alkali feldspars [1].

The Eocene facies in northeast of the study area, i.e. in Shast Darreh mountains is different with the other facies in the area, and it starts with light grey conglomerates involving limestone elements of Cretaceous period and occasionally andesite. This conglomerate unit is covered by thick green tuff interbedded with limestone and marl, in which fossils with middle Eocene age can be observed [1].

After Eocene, the Taknar zone is often recognized by granodiorite and diorite units in volcanic and pyroclastic rocks with Paleogene age in northern and central parts of Feizabad area. The largest plutonic body composed of a granodiorite unit is observed in north of Azghand. Northern margin of this granodiorite unit is formed of granite. These rocks are characterized by their coarse grains and porphyry texture [1]. The geological map of Torbat-e-Heydarieh area has been shown in Figure 1.

3. Discussion

3.1. Conditional probability and weights of evidence modeling

The method of WOFE is a data-driven method that integrates a variety of exploring data. This method is the logarithmic-linear form of Bayesian probability model in estimating the relative importance of each evidence using statistical tools.

The approach generally uses Dichotomous maps, and the generalization and reclassification of geo data into dichotomous maps may result in distortion and possible loss of valuable information. Moreover, reclassification rules are based on available information and these rules may change as more information becomes available [3]. The model was originally developed for mineral potential assessment [4-12].

The approach involves extraction of dichotomous predictor patterns based on the quantified spatial correlation between a set of relevant factors and events [13].

In mineral exploration applications of the method, a series of evidential maps from geochemical, geophysical, geological and other exploration data are obtained. These maps or data are used to obtain final mineral prospect or promising map in which prospect areas or zones have been determined. Spatial dependence of each evidential map with respect to known mineral deposits of the type sought is computed and used as the training dataset [14].

The WOFE method is based on Bayes' rule, in which from the weighted integrated map, we can obtain an optimally-predicted pattern for mineral potential or prospectivity mapping in regional scale. For this prediction, spatial correlations between known mineral deposits of the type is sought and related factor (e.g. geochemistry, alteration, structure, geology, airborne geophysics) are computed, and then, two weights, i.e. w_+ and w_- , are determined for each predicted pattern. These weights are used as criteria for recognition of new mineral deposits.

According to Bayes' rule, a binary hypothesis is tested when a certain domain (binary predictor pattern) is present (Equation 1) or absent (Equation 2).

$$P(D/B) = \frac{P(D \cap B)}{P(B)} = P(D) \frac{P(B/D)}{P(B)} \quad (1)$$

$$P(D/\bar{B}) = \frac{P(D \cap \bar{B})}{P(\bar{B})} = P(D) \frac{P(\bar{B}/D)}{P(\bar{B})} \quad (2)$$

Where P is probability, B is the presence of dichotomous pattern, \bar{B} is the absence of dichotomous pattern, D is the presence of event occurrence. W+ and W- are the weights-of-evidence when a factor is present (relevant) and absent (not relevant), respectively [7, 9].

Scoring performed on that domain and a known event (e.g. the presence of a mineral occurrence) results in (1) W+ weights within the test domain and

(2) W-weights not within the test domain. The weights for binary patterns are:

$$W^+ = \text{Log}_e \frac{P(B/D)}{P(\bar{B}/D)} \quad (3)$$

$$W^+ = \text{Log}_e \frac{P(B/D)}{P(\bar{B}/D)} \quad (4)$$

$$W^- = \text{Log}_e \frac{P(\bar{B}/D)}{P(B/D)} \quad (5)$$

$$C = W^+ - W^- \quad (6)$$

Where W+ is the weight when the binary map B presents and W- is the weight when the binary map B is absent. The contrast C quantifies the spatial correlation between each binary map and the known events.

In the case of a large number of mineral occurrences, for each test domain, the maximum contrast often gives the best measure of spatial correlation with the mineral occurrence points [9]. In the case of a small area and a small number of mineral occurrences, the uncertainty of the weights can be large and C can be meaningless and the studentized value of C, calculated as the

ratio of C to its standard deviation, C/s(C), serves as a test that the spatial correlation between the mineral occurrence points and a test domain is statistically significant [9]. The standard deviation of C is the square root of the sum of the variances of the weights. The studentized value of C is used to define the optimum cutoff [6, 8].

$$S_c = \sqrt{s^2(W^+) + s^2(W^-)} \quad (7)$$

$$\text{Sig}C = C / \sqrt{s^2(W^+) + s^2(W^-)} \quad (8)$$

These procedures are implemented in a GIS. Binary maps (test domains), representing the seven deposit recognition criteria, are generated and for each map the weights are calculated (i.e., a value of W+ for presence and of W- for absence) at every location (pixel). Then the weighted binary maps are combined to create a final predictive map [7, 9].

In this study, seven maps representing favorable geology, aeromagnetic, geochemistry, proplite alteration, iron oxides alteration, hydroxyl-bearing minerals and structure features were created and used for WOFE analysis.

3.2. Analysis of geology

Lithological map of the study area was obtained on the basis of 1:100000 scale geological map of the area. As a result, 7 types of lithologies, in which mineralization exists, were selected for the computations in the method of weights of evidence. Based on the obtained results, shown in Table 1, 5 out of these 7 types of lithologies were evaluated as favorable for mineralization, and were used in the integration process.

Table 1. Weights of evidence analysis of the favorable geological lithologies.

Lithology	Area (Km ²)	Min. points	w+	w-	C	Sig C	s (w+)	s (w-)	Sc
Ebt	201.042	15	1.153	-0.618	1.77	6.715	0.066	0.002	0.26
Tgd	140.309	6	0.588	-0.119	0.708	1.700	0.167	0.006	0.42
Tal	12.245	1	1.245	-0.027	1.272	1.245	1.005	0.038	1.02
Etv	22.508	2	1.332	-0.057	1.389	1.922	0.502	0.019	0.72
Td	2.664	1	2.848	-0.035	2.884	2.798	1.024	0.038	1.03
Etm	64.877	1	-0.438	0.021	-0.459	-0.450	1.001	0.038	1.02
Et	27.859	1	0.412	-0.012	0.425	0.416	1.002	0.038	1.02

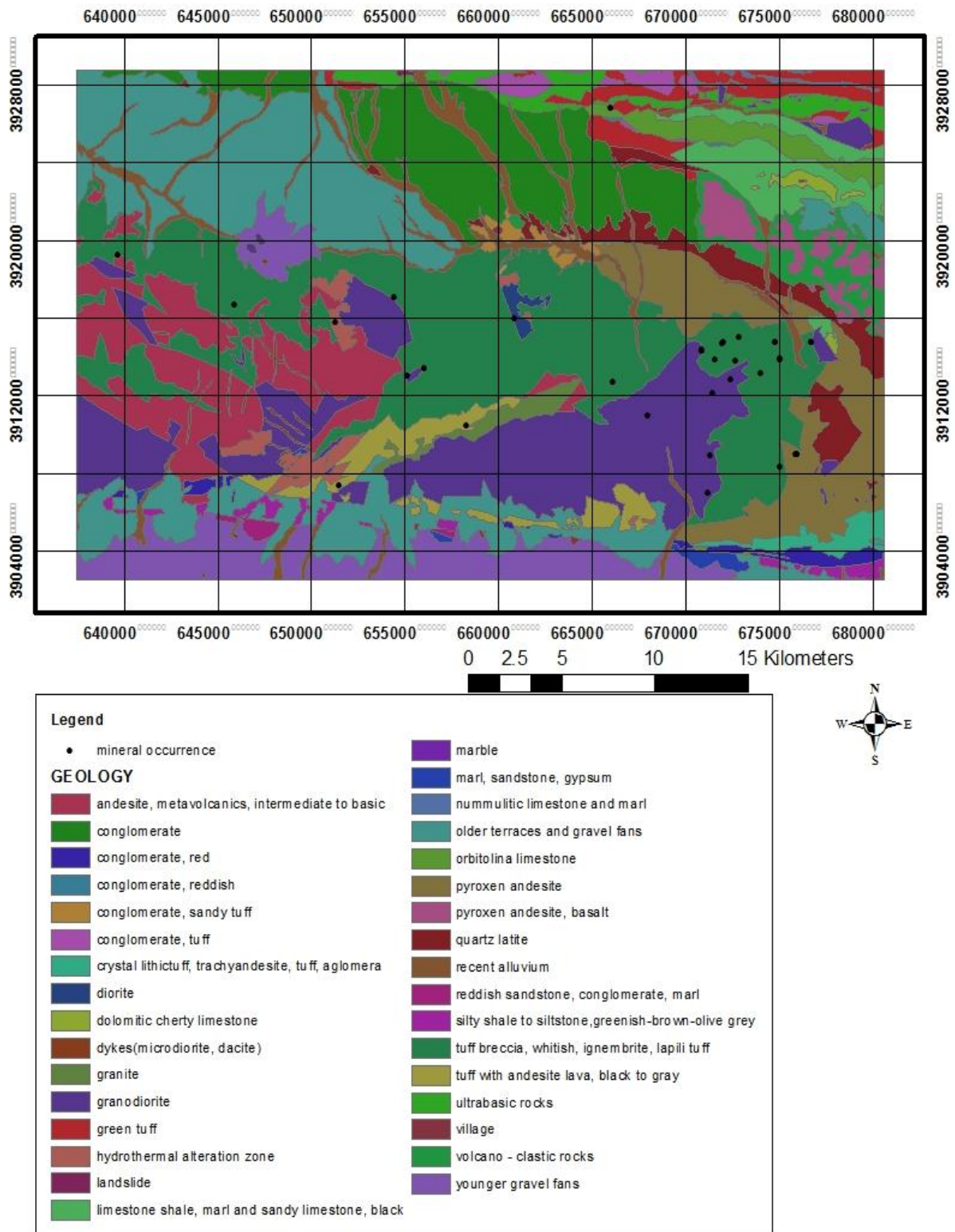


Figure 1. 1:100,000 scale geological map of Torbat-e-Heydarieh area.

Where

Ebt: White tuff breccias, iignem brite, green lapili tuff and sandy tuff

Tgd: Granodiorite

Tal: Hydrothermal alteration zone

Etv: Tuff with andesitic lava, black to grey

Td: Diorite

Etm: Pyroxen andesite

Et: Green tuff

3.3. Analysis of aeromagnetic data

The researchers used 1:250000 scale aeromagnetic data and maps to assess geomagnetic characteristics of the area. Following aeromagnetic data processing and interpretation, high intensity magnetic zones and also magnetic structures in the subsurface was recognized in the related magnetic maps. As a result, one can observe that granodiorite belt and pyroxene andesite and basalt units in 1:100000 scale Feizabad geological map coincide with high magnetic intensities (Figure 2).

Applying various magnetic filters on the magnetic data demonstrated that the magnetic anomalies continue in deeper parts of the subsurface, and

also, it is inferred that granitoid zone is more extensive in these deeper parts, and this zone has just a limited outcrop in the surface of the area.

Based on the magnetic intensities in the magnetic map, the area is classified into 9 different magnetic zones, and then, WOFE computations or analyses are made on these 9 zones. The results of this analysis are shown in Table 2. Among these 9 magnetic data ranges, only two magnetic data ranges have been evaluated as suitable for gold exploration. Granodiorite intrusions have high magnetic values. Porphyry deposits are often around these masses then two magnetic data ranges were correctly evaluated as suitable area based on WOFE method.

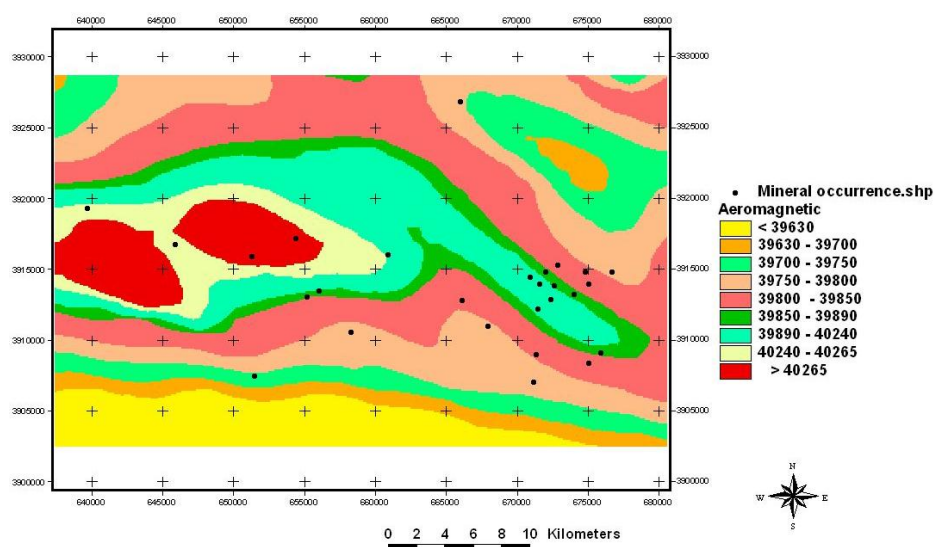


Figure 2. 1:250,000 scale aeromagnetic map of Torbat-e-Heydarieh area.

Table 2. Weights of evidence analysis of the favorable aeromagnetic zones.

Magnetic (nt)	Area (Km ²)	Min. points	w+	w-	C	Sig C	s (w+)	s (w-)	Sc
>40265	72.826	2	0.14	-0.01	0.15	0.21	0.50	0.02	0.72
40240-40265	69.025	2	0.20	-0.01	0.21	0.29	0.50	0.02	0.72
39890-40240	152.111	5	0.32	-0.06	0.38	0.84	0.20	0.01	0.46
39850-39890	74.579	5	1.04	-0.14	1.18	2.59	0.20	0.01	0.46
39800-39850	266.926	7	0.10	-0.03	0.13	0.33	0.14	0.01	0.39
39750-39800	213.162	5	-0.02	0.00	-0.02	-0.04	0.20	0.01	0.46
39700-39750	125.744	1	-1.10	0.08	-1.18	-1.16	1.00	0.04	1.02
39630-39700	54.417	0	-	-	-	-	-	-	-
<39630	106.009	0	-	-	-	-	-	-	-

3.4. Analysis of structures

The faults, which had spatial association with known mineralization in the area, were digitized from the 1:100,000 scale geologic map of the area. To estimate WOFE of different categories of the structural map (Table 3), the structural map

was also rasterized, and then, buffered at distances of 200 m to 800 m and crossed with the raster mineral occurrence point map. The optimum buffer, which resulted in the maximum studentized value of C, was considered to be 200

m. The resulting buffered structural domain covers 28% of the area, and also, 10 out of 27 mineral occurrences are present in this zone (Figure 3).

Analysis of the WOFE reveals a correlation between the structural map and mineral

occurrences. The weights used in the final model are:

W+=0.27 if in a favorable structural domain

W-=-0.13 if not in a favorable structural domain

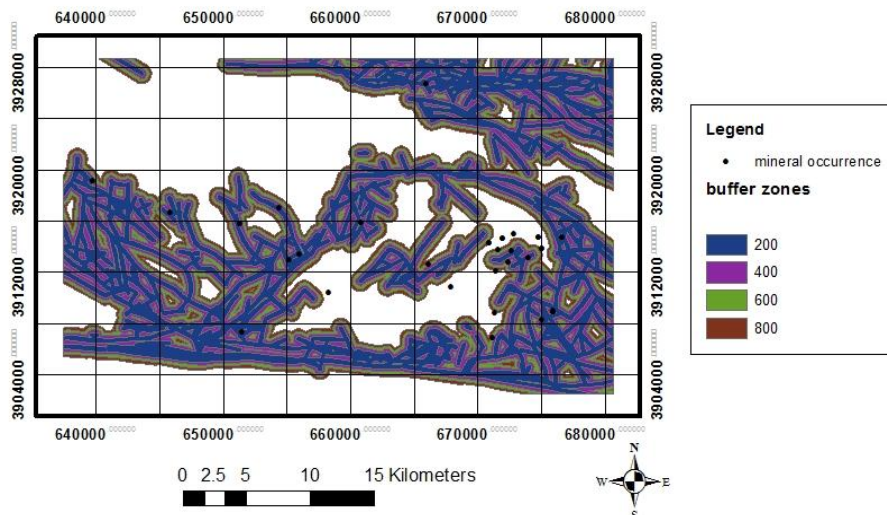


Figure 3. Map of structural domain with the buffer zones and mineral occurrence points.

Table 3. Weights of evidence analysis of different categories of the structural domain.

Buffer (m)	Area (Km ²)	Min. points	w+	w-	C	Sig	s (w+)	s (w-)	Sc
200	319.822	10	0.27	-0.13	0.40	1.25	0.10	0.00	0.32
400	186.163	4	-0.10	0.02	-0.12	-0.24	0.25	0.01	0.51
600	111.530	3	0.12	-0.01	0.14	0.23	0.33	0.01	0.59
800	79.227	1	-0.64	0.04	-0.67	-0.66	1.00	0.04	1.02

3.5. Analysis of geochemical data

The stream sedimentary samples in the study area were analyzed. We have considered the samples with Au assay values of more than 2.5 ppb as anomalies. In general, anomalous assay values

were classified into three categories. Based on the obtained results, we can use the geochemical data to map and recognize mineral potentials in the study area, as indicated in Figure 4 and Table 4.

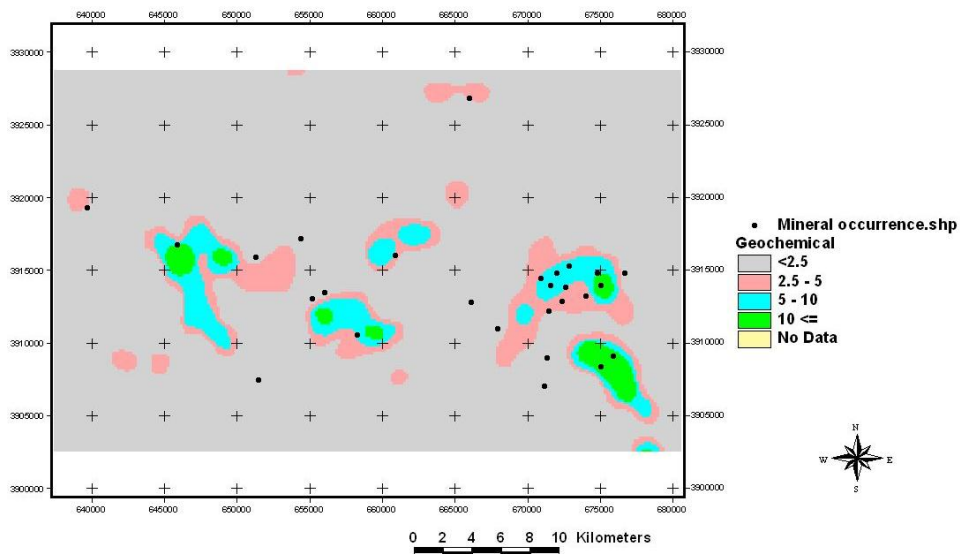


Figure 4. Geochemical anomaly map of Torbat-e-Heydarieh area and mineral occurrence points.

Table 4. Weights of evidence analysis of the favorable geochemical zones.

Au (ppb)	Area (Km ²)	Min. points	w+	w-	C	Sig c	s (w+)	s (w-)	Sc
>= 10	17.370	5	2.56	-0.19	2.75	5.98	0.20	0.01	0.46
5_ 10	49.286	5	1.47	-0.16	1.63	3.56	0.20	0.01	0.46
2.5_ 5	85.227	6	1.09	-0.17	1.27	3.04	0.17	0.01	0.42

3.6. Analysis of argillic alteration

Argillic zones that can be recognized as a result of processing remote sensing data, considering the chemical composition of this alteration and also its extents on the surface of the study area, are very important as these alteration zones can be used as guidance for recognizing mineralization types. In general, remote sensing data can be used to prospect and exploration of mineral deposits [15].

In this study, alteration zones were identified using Aster data. A suitable Aster spectral range was selected to detect the main alteration mineral spectral features. The instrument consists of three separate subsystems with a total of 14 bands [16, 17].

Clay minerals have high reflectance in band 4 and high absorption in band 5 and 6 [18-22].

Argillic alteration was identified using 4/(5+6) ratio band. The resulting argillic alteration map was buffered at distances of 100 to 400 meters, crossed with the raster mineral occurrence map (Figure 5) and weights of evidence, contrast C and studentized values of C were calculated (Table 5). The optimum buffers, which yield the maximum studentized value of C, were defined at 300 and 400 meters of the argillic alteration zones.

The WOFE analysis reveals a correlation between the argillic alteration and mineral occurrences (Table 5).

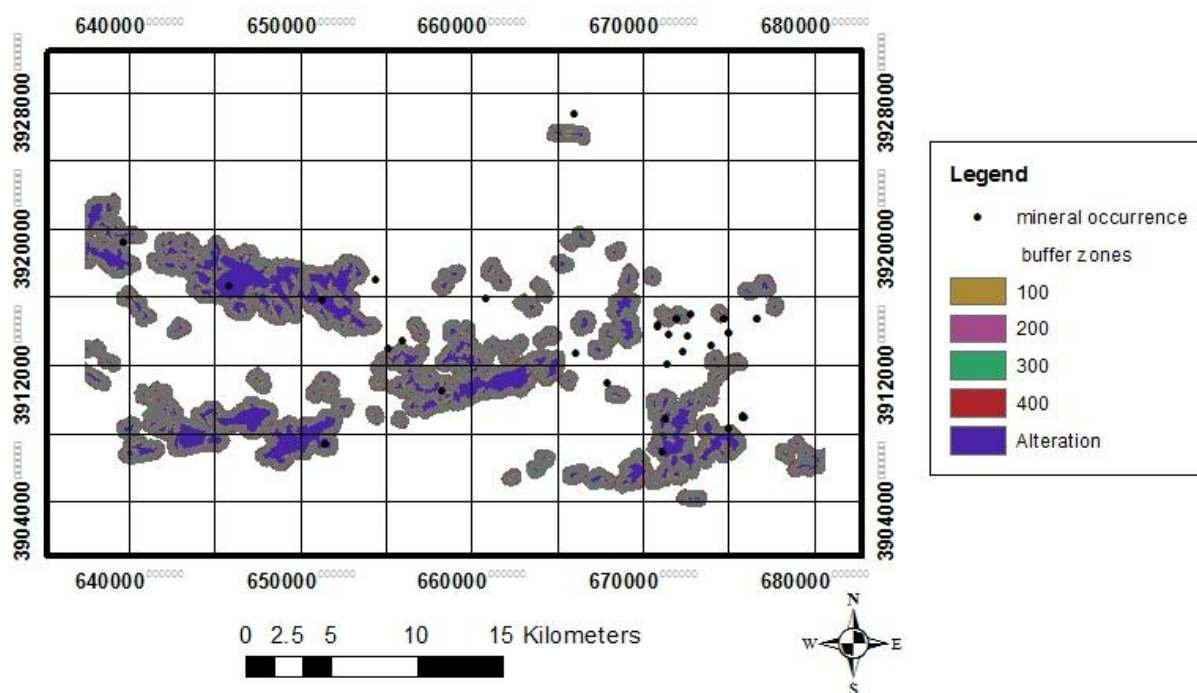


Figure 5. Map of argillic alteration domain with the buffer zones and mineral occurrence points.

Table 5. weights of evidence analysis of the favorable argillic alteration zones.

Buffer(m)	Area (Km ²)	Min. points	w+	w-	C	Sig c	s (w+)	s (w-)	Sc
100	44.881	0	-	-	-	-	-	-	-
200	40.938	1	0.02	0.00	0.03	0.02	1.00	0.04	1.02
300	38.757	2	0.78	-0.04	0.82	1.14	0.50	0.02	0.72
400	37.436	2	0.81	-0.04	0.86	1.19	0.50	0.02	0.72
Alteration	61.030	5	1.25	-0.15	1.40	3.06	0.20	0.01	0.46

3.7. Analysis of propillitic alteration

Propillitic alteration was also identified in the study area. Chlorite and epidote minerals have high reflectance in bands 6 and 9, and high absorption in bands 7 and 8 [18- 22].

Propillitic alteration was determined using (6+9)/(7+8) ratio band.

The resulting propillitic alteration domain map was buffered at distances of 100 m to 400 m, crossed with the raster mineral occurrence map

(Figure 6) and weights of evidence, contrast C and studentized values of C were calculated (Table 6). The optimum buffers, which yield the maximum studentized value of C, were defined at 100, 200, 300 and 400 meters of the propillitic alteration zones.

The weights of evidence analysis reveals a strong correlation between the propillitic alteration and mineral occurrences as can be seen from Table 6.

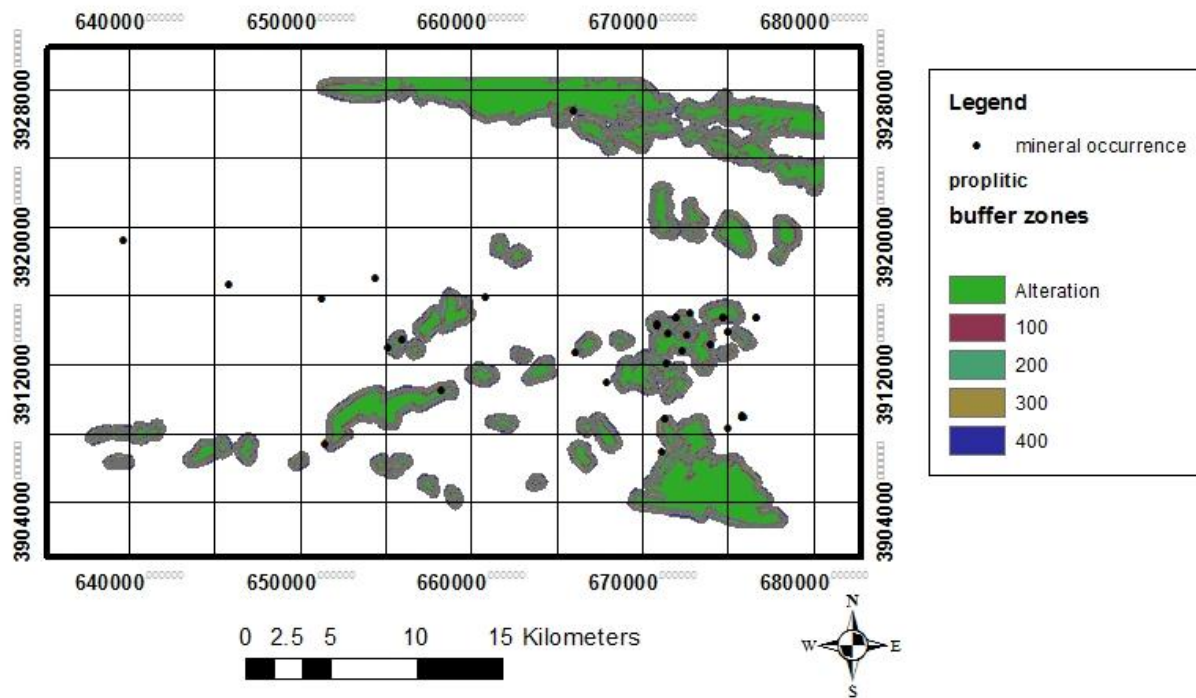


Figure 6. Map of proplitic alteration domain with the buffer zones and mineral occurrence points.

Table 6. Weights of evidence analysis of the favorable proplitic alteration domain.

Buffer (m)	Area (Km ²)	Min. points	w+	w-	C	Sig c	s (w+)	s (w-)	Sc
100	34.358	2	0.90	-0.05	0.95	1.31	0.50	0.02	0.72
200	33.691	3	1.33	-0.09	1.42	2.41	0.34	0.01	0.59
300	32.591	4	1.66	-0.13	1.80	3.51	0.25	0.01	0.51
400	31.733	5	1.92	-0.18	2.10	4.59	0.20	0.01	0.46
Alteration	87.009	2	-0.04	0.00	-0.04	-0.06	0.50	0.02	0.72

3.8. Analysis of iron oxide alteration

Iron oxide alterations have high reflection in band 2 and high absorption in band 1 of Aster images [18-22].

Iron oxide alteration zones were identified using 2/1 band ratio in this area. The resulting iron oxide alteration domain map was buffered at distances of 100 to 400 meters, crossed with the raster mineral occurrence map (Figure 7) and

weights of evidence, contrast C and studentized values of C were calculated (Table 7). The optimum buffers, which yield the maximum studentized value of C, were defined at 200 meters of the iron oxide alteration zones.

The WOFE analysis revealed a strong correlation between the iron oxide alteration and mineral occurrences as shown in Table 7.

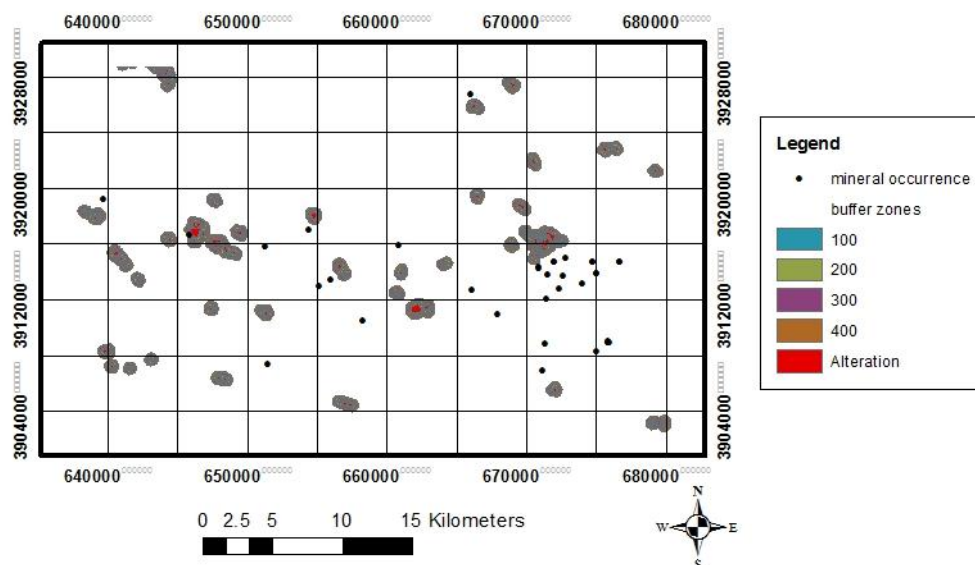


Figure 7. Map of iron oxide alteration domain with the buffer zones and mineral occurrence points.

Table 7. Weights of evidence analysis of the favorable iron oxide alteration zones.

Iron oxid	Area (km2)	Min. points	w+	w-	C	Sig C	s (w+)	s (w-)	Sc
100	8.744	0	-	-	-	-	-	-	-
200	10.349	1	1.42	-0.03	1.45	1.42	1.01	0.04	1.02
300	12.004	0	-	-	-	-	-	-	-
400	13.803	0	-	-	-	-	-	-	-
Alteration	3.765	0	-	-	-	-	-	-	-

4. Data integration

Having made WOFE calculations and obtaining mineral potential maps based on primary mineral exploration data, all the mineral potential maps were integrated to produce the final predictive mineral potential map in which the probability of mineralization in different parts of the map has been computed. As a result, post probability of gold mineral occurrences in the study area was determined (Figure 8). Therefore, considering the map shown in this Figure, 4 prospect areas or zones with considerable mineralization are recognized. These 4 prospect areas are sorted based on exploration preference or priority from areas 1 to 4 as introduced in the following:

Area 1: In this area, various kinds of mineralization can be seen that may or may not be accompanied by gold mineralization with different concentrations. Two types of hypogen gold mineralization in Kuh Zar gold deposit are:

Specularite + quartz + gold and Specularite + quartz + chalcopyrite ± pyrite + gold

Mineralization texture is often in the forms of breccia and veinlet to stock work, and rarely is of massive vein type. This prospect area is the most significant area from the view points of mineralization intensity, assay and reserve estimation value.

Area 2: In this area, sulphide mineralization (pyrite and chalcopyrite) with disseminated texture or form, and occasionally veinlet form in porphyry plutonic stocks or surrounding rocks, is observed. Furthermore, in some parts of the area, we can observe sheeted vein and semi-parallel thin veinlet systems where strong acid leaching has occurred in the surrounding rocks. The mineralization in these thin veinlets is quartz, secondary iron oxide, and so on. Secondary copper mineralization comprising of malachite and occasionally azurite in west and southwest of this area can be observed. This secondary copper mineralization occurs in joints and fractures of the volcanic rocks in the area and the mineralization is accompanied with slight amounts of fine-grained chalcopyrite traces that are scattered in the volcanic host rock. In west to northwest of the area, an extensive set, composed of silica veins and veinlets with enriched secondary iron oxide, is observed.

Area 3: In this area, sulfide mineralization comprising of chalcopyrite, galena and pyrite is observed in the form of veins. The mineralization has an outcrop with a length of about 200 meters and approximate vertical dip. In some parts of the area, the thickness of the veins reaches to 6

meters, and the gold concentration has been reached to 7.8 ppm.

Area 4: In this area, vein and veinlet forms of mineralization in faulting zones are observed. The mineralization is often composed of silica veins and veinlets with specularite, chalcopyrite, pyrite, and slightly galena minerals accompanied by gangue quartz mineral. Abundant of silica veinlets

in rock units is the main characteristic of this area so that veinlet zones in many parts of the area such as Siano Mountain are formed. These veinlets are occasionally accompanied with specularite, copper sulfide and of pyrite mineralization. In a part of the area, the gold concentration has been reached to 36 ppm.

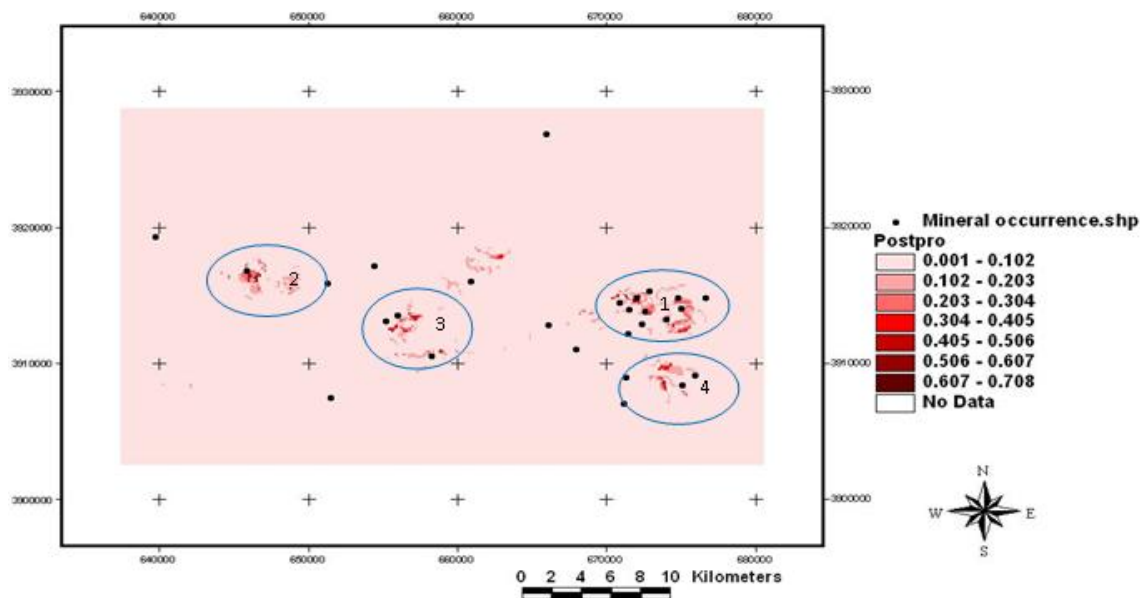


Figure 8. Map of post probability of gold mineral occurrences in the Torbat Haydarieh area.

5. Conclusions

In this study, the method of WOFE was applied to obtain gold potential map based on airborne geophysical, geological, structural, remote sensing, and geochemical data or maps, and also, 27 known gold mineralized locations in Torbat-e-Heydarieh area. These exploratory maps were integrated to produce the final predictive mineral potential map. The interesting results were obtained using this GIS model. As a result, 4 gold mineralization areas or zones with different mineralization post probability values were recognized in the study area. These mineralization zones were also confirmed following field checking or visit of the study area. These 4 target areas desirably include the variety of mineralization elements. This research shows that the method of WoFE is an effective technique for the exploration and evaluation of regional-scale mineral deposits.

References

[1]. Heydari, A. (2011). Exploration report of Kuh Zar deposit in Torbat-e-Heydarieh area, Zarmehr mining company, 133 p.

[2]. Ford, A., and Blenkinsop, T.G. (2008). Combining fractal analysis of mineral deposit clustering with weights of evidence to evaluate patterns of mineralization: application to copper deposits of the Mount Isa Inlier, NW Queensland, Australia. *Ore Geology Reviews*, 33 (3): 435-450.

[3]. Porwal, A.K. (2006). Mineral potential mapping with mathematical geological models. ITC PhD Dissertations, 130 p.

[4]. Agterberg, F.P., Bonham-Carter, G.F. and Wright, D.F. (1990). Statistical pattern integration for mineral exploration. Computer applications in resource estimation prediction and assessment for metals and petroleum: Pergamon Press, Oxford, 1-21.

[5]. Agterberg, F.P., Bonham-Carter, G.F., Cheng, Q. and Wright, D.F. (1993). Weights of evidence modeling and weighted logistic regression for mineral potential mapping. *Computers in geology*, 25: 13-32.

[6]. Alok, P. and Hale, M. (2000). GIS based weights of evidence analysis of multi class spatial data for predictive mineral mapping: a case study from Aravalli province, western India. Proceeding Fourteenth International Conference on Applied Geologic Remote Sensing, Las Vegas, Nevada. Veridian (ERIM International: Ann Arbor), 377-384.

- [7]. Asadi, H.H. and Hale, M. (2001). A predictive GIS model for mapping potential gold and base metal mineralization in Takab area, Iran. *Computers & Geosciences*, 27 (8): 901-912.
- [8]. Bonham-Carter, G.F., Agterberg, F.P. and Wrigh, D.F. (1989). Weights of evidence modeling: a new approach to mapping mineral potential. In: Agterberg, F.P., Bonham-Carter, G. F. (Eds.), *Statistical Applications in the Earth Sciences: Geol. Surv. Of Canada, Paper*, 89 (9): 171–183.
- [9]. Bonham-Carter, G.F. (1994). *Geographic information systems for geoscientists: modelling with GIS* (Vol. 13). Access Online via Elsevier.
- [10]. Carranza, E.J. M. and Hale, M. (2000). Geologically constrained probabilistic mapping of gold potential, Baguio district, Philippines. *Natural Resources Research*, 9 (3): 237-253.
- [11]. Harris, J.R., Wilkinson, L. and Grunsky, E.C. (2000). Effective use and interpretation of lithogeochemical data in regional mineral exploration programs: application of Geographic Information Systems (GIS) technology. *Ore Geology Reviews*, 16 (3): 107-143.
- [12]. Venkataraman, G., Madhavan, B.B., Ratha, D.S., Antony, J.P., Goyal, R.S., Banglani, S. and Roy, S.S. (2000). Spatial modeling for base-metal mineral exploration through integration of geological data sets. *Natural Resources Research*, 9 (1): 27-42.
- [13]. Oh, H.J. and Lee, S. (2010). Assessment of ground subsidence using GIS and the weights-of-evidence model. *Engineering Geology*, 115 (1): 36-48.
- [14]. Kempt, L., Bonham-carter, G.F. and Raines, G. L. (1999). Arc-Wofe: Arcview extention for weights of evidencemapping.
- [15]. Floyd Sabin, J. R. (2007). *Remote Sensing: Principles and Interpretation*, Waveland Pr Inc, 512 p.
- [16]. Di Tommaso, I. and Rubinstein, N. (2007). Hydrothermal alteration mapping using ASTER data in the Infiernillo porphyry deposit, Argentina. *Ore Geology Reviews*, 32 (1): 275-290.
- [17]. Fujisada, H., Iwasaki, A. and Hara, S. (2001). ASTER stereo system performance. In *International Symposium on Remote Sensing* (pp. 39-49). International Society for Optics and Photonics.
- [18]. Grove, C.I., Hook, S.J. and Paylor III, E.D. (1992). Laboratory reflectance spectra of 160 minerals, 0.4 to 2.5 micrometers.
- [19]. Hewson, R.D., Cudahy, T.J., Mizuhiko, S., Ueda, K. and Mauger, A.J. (2005). Seamless geological map generation using ASTER in the Broken Hill-Curnamona province of Australia. *Remote Sensing of Environment*, 99 (1): 159-172.
- [20]. Hunt, G.R. and Salisbury, J.W. (1971). Visible and near infrared spectra of minerals and rocks. II. Carbonates. *Modern Geology*, 2: 23-30.
- [21]. Salisbury, J.W. and D'Aria, D.M. (1992). Emissivity of terrestrial materials in the 8–14 μm atmospheric window. *Remote Sensing of Environment*, 42 (2): 83-106.
- [22]. Vicente, L.E. and de Souza Filho, C.R. (2011). Identification of mineral components in tropical soils using reflectance spectroscopy and advanced spaceborne thermal emission and reflection radiometer (ASTER) data. *Remote Sensing of Environment*, 115 (8): 1824-1836.

مدل وزن‌های نشانگر در GIS برای تهیه نقشه پتانسیل معدنی ذخایر طلای هیدروترمال در منطقه تربت حیدریه

حسین شاهی*، ابوالقاسم کامکار روحانی

دانشکده مهندسی معدن، نفت و ژئوفیزیک، دانشگاه شاهرود، ایران

ارسال ۲۰۱۲/۵/۱۹، پذیرش ۲۰۱۴/۹/۶

* نویسنده مسئول مکاتبات: hssn.shahi@gmail.com

چکیده:

روش وزن‌های نشانگر یکی از روش‌های مهم داده محور جهت تعیین نقشه پتانسیل مطلوب معدنی در GIS است. در این روش با توجه به ویژگی‌های مناطق کانی‌سازی شناخته‌شده، مناطق کانی‌سازی جدید می‌توانند مورد شناسایی قرار گیرند. در این مطالعه روش وزن‌های نشانگر جهت تهیه نقشه پتانسیل معدنی طلای هیدروترمال در منطقه تربت حیدریه در شرق ایران مورد استفاده قرار گرفت. بر اساس تعداد نسبتاً زیاد شواهد معدنی شناخته‌شده (۲۷ منطقه کانی‌سازی شناخته‌شده طلا) که در منطقه شناسایی شده است، استفاده از روش وزن‌های نشانگر برای اکتشاف مناطق جدید معدنی طلا در این منطقه می‌تواند بسیار کارآمد باشد. جهت تعیین نقشه کانی‌سازی احتمالی به صورت نقشه احتمال متأخر بر اساس روش وزن‌های نشانگر، نتایج داده‌های مغناطیس‌هوایی، زمین‌شناسی، آلتراسیون‌های آرژلیک، پروپیلیتیک و اکسید آهن، داده‌های ژئوشیمی و ساختاری با یکدیگر تلفیق شده‌اند. بر این اساس چهار منطقه اصلی در این محدوده به عنوان مناطق دارای پتانسیل بالای کانی‌سازی طلا مورد شناسایی قرار گرفتند که دارای رگه‌ها و رگچه‌های کانی‌سازی می‌باشند.

کلمات کلیدی: سیستم اطلاعات جغرافیایی (GIS)، کانی‌سازی طلا، مدل وزن‌های نشانگر، نقشه پتانسیل معدنی، احتمال شرطی.